



OPEN

Upregulated LAMA3 modulates proliferation, adhesion, migration and epithelial-to-mesenchymal transition of cholangiocarcinoma cells

Kittiya Islam¹, Brinda Balasubramanian¹, Simran Venkatraman², Parichut Thummarati³, Janpen Tunganuntarat¹, Nut Phueakphud¹, Phongthon Kanjanasirirat⁴, Tanawadee Khumpanied⁴, Pornparn Kongpracha¹, Yingpinyapat Kittirat^{5,6,7}, Rutaiwan Tohtong¹, Tavan Janvilisri¹, Patompon Wongtrakoongate^{1,8}, Suparek Borwornpinyo^{4,9}, Nisana Namwat^{5,6,10} & Tuangporn Suthiphongchai¹✉

A poor outcome for cholangiocarcinoma (CCA) patients is still a clinical challenge. CCA is typically recognized by the desmoplastic nature, which accounts for its malignancy. Among various extracellular matrix proteins, laminin is the most potent inducer for CCA migration. Herein, we accessed the expression profiles of laminin gene family and explored the significance of the key laminin subunit on CCA aggressiveness. Of all 11 laminin genes, LAMA3, LAMA5, LAMB3 and LAMC2 were concordantly upregulated based on the analysis of multiple public transcriptomic datasets and also overexpressed in Thai CCA cell lines and patient tissues in which LAMA3A upregulated in the highest frequency (97%) of the cases. Differential expression genes (DEGs) analysis of low and high laminin signature groups revealed LAMA3 as the sole common DEG in all investigated datasets. Restratifying CCA samples according to LAMA3 expression indicated the association of LAMA3 in the focal adhesion pathway. Silencing LAMA3 revealed that it plays important roles in CCA cell proliferation, adhesion, migration and epithelial-to-mesenchymal transition. Taken together, this research signifies the roles of dysregulated ECM homeostasis in CCA malignancy and highlights, for the first time, the potential usage of LAMA3 as the diagnostic biomarker and the therapeutic target to tackle the CCA stromal.

Cholangiocarcinoma (CCA), the epithelial cancer of bile ducts, is relatively rare but notoriously lethal with the highest reported global incidence in northeastern Thailand. Combination of silent symptom with diagnostic delay, poor prognosis and chemoresistance contributes to an alarming raise in the global mortality of CCA yearly¹. The aggressiveness of CCA is not only a consequence of the neoplastic cells themselves, but also a result of tumor microenvironment (TME) created by the extensive remodeling of extracellular matrix (ECM) constituents and the reciprocal communication between cancerous cells and the authoritative tumor stromal cells². During

¹Department of Biochemistry, Faculty of Science, Mahidol University, Bangkok 10400, Thailand. ²Graduate Program in Molecular Medicine, Faculty of Science, Mahidol University, Bangkok 10400, Thailand. ³Department of Clinical Chemistry, Faculty of Allied Health Sciences, Chulalongkorn University, Bangkok 10330, Thailand. ⁴Excellent Center for Drug Discovery (ECDD), Faculty of Science, Mahidol University, Bangkok 10400, Thailand. ⁵Department of Biochemistry, Faculty of Medicine, Khon Kaen University, Khon Kaen 40002, Thailand. ⁶Cholangiocarcinoma Research Institute, Khon Kaen University, Khon Kaen 40002, Thailand. ⁷Present address: Department of Medical Sciences, Regional Medical Sciences Center 2, Ministry of Public Health, Phitsanulok 65000, Thailand. ⁸Center for Neuroscience, Faculty of Science, Mahidol University, Bangkok 10400, Thailand. ⁹Department of Biotechnology, Faculty of Science, Mahidol University, Bangkok 10400, Thailand. ¹⁰Present address: Department of Systems Biosciences and Computational Medicine, Faculty of Medicine, Khon Kaen University, Khon Kaen 40002, Thailand. ✉email: tuangporn.sut@mahidol.ac.th

CCA progression and metastasis, the surrounding ECM experiences significant biological and architectural alterations, including increased secretion of ECM proteins, such as collagens, fibronectins, laminins, periostin and tenascin-C³. These phenomena take part in the pathogenesis of CCA via several mechanisms involving in accelerating migration and invasion, evading immune destruction, and inducing angiogenesis⁴.

Understanding ECM roles and how disruption of ECM dynamics influences cancer development, and progression may shed the light on the improvement of early detection and promising treatment for patients with CCA. Laminins, a large family of heterotrimeric glycoproteins, assemble into cross-like structures from different combinations of five α (LAMA1–5), three β (LAMB1–3) and three γ (LAMC1–3) chains. At least 16 isoforms of laminins have been identified and accordingly named based on their chain composition; for instance, laminin-332 (formerly laminin-5) comprises $\alpha 3$, $\beta 3$ and $\gamma 2$ chains⁵. A wide variation in their biological roles is presumably mediated through their receptor repertoires, mainly integrins; for example, integrin $\alpha 6\beta 4$ binding increase cell motility and proliferation through the activation of JNK cascade via Rac 1 or Ras/Raf/MAPK pathway, while integrin $\alpha 6\beta 1$ binding causes tyrosine phosphorylation of p190RhoGAP, and thus stimulates protrusive and degradative activities necessary for invasion^{6,7}. Copious amount of evidence has reported the aberrant expression of laminins and their association with biological characteristics and clinical outcomes of several types of cancers, such as colon, kidney, liver, lung and stomach⁷.

Epithelial-to-mesenchymal transition (EMT) is a reversible cellular program which transiently transforms epithelial cells into mesenchymal phenotypes and behaviors. During EMT, epithelial cells encounter specific signals from their microenvironment to trigger (i) the reorganization of cytoarchitecture into fibroblast-like morphology, (ii) the downregulated expression of intercellular junction proteins, such as claudin-1, E-cadherin and zonula occludens-1 and (iii) the upregulation of mesenchymal markers, namely fibronectin, N-cadherin and vimentin. Concurrently, these phenomena loosen cell–cell adhesion, alter cell–matrix interaction and ameliorate migratory capacity, apoptosis resistance and ECM degradation, which are crucial processes for cancer metastasis⁸.

Alteration of the ECM in CCA plays several roles in malignancy behaviors. These roles include promoting cell proliferation, migration, metastasis, EMT, angiogenesis, fibrosis, and ECM stiffness. Additionally, it weakens basement membrane integrity, recruits inflammatory cells and myofibroblasts, and serves as reservoirs for cytokines and growth factors that affect cancer progress⁹. Several types of alterations, such as overexpression of periostin or tenascin C, correlate with metastasis and short survival of CCA patients⁹. Due to the complex relationship between TME and the enhanced malignant behaviors of CCA, the significance of ECM proteins in the pathogenesis of CCA still needs to be addressed. Among a variety of evaluated ECM proteins, laminin shows the highest ability in enhancing CCA cell migration and the overexpressed LAMB1 is correlated with lymphatic invasion¹⁰. Suppression of LAMB3 expression by microRNA-329 inhibits EMT and lymph node metastasis in CCA¹¹. Upregulation of LAMC2 expression in CCA is associated with CCA malignancy^{12,13}. Up to our knowledge, however, relatively little is known about the expression of laminin gene family and their contribution to CCA progression as well as the potential usage as CCA biomarkers.

In the current study, we utilized multiple publicly available datasets containing transcriptomic data of CCA tissues to investigate the expression of laminin gene family. We also validated these results in tissues and cell lines of Thai CCA patients. Furthermore, we identified LAMA3 as the uniquely upregulated laminin in CCA and further explored its functions and a novel molecular mechanism of action in CCA progression. Our finding underlines the gravity of dysregulated cell-ECM interaction in CCA malignancy and suggests the optimistic prospect in using LAMA3 not only as the diagnosis biomarker for CCA but also as the therapeutic strategy for desmoplastic CCA therapy.

Results

Expression profiling of laminin gene family in CCA through publicly available databases

To examine the differential expression of laminin gene family in CCA, the basal mRNA expression levels of LAMA1-5, LAMB1-3 and LAMC1-3 were obtained from three RNA-seq datasets retrieved from GEO, TCGA and PCAWG. The GSE107943 dataset obtained from GEO revealed nine overexpressed laminin genes in CCA compared to the adjacent noncancerous tissues, namely LAMA2, LAMA3, LAMA4, LAMA5, LAMB1, LAMB2, LAMB3, LAMC1, and LAMC2 (Fig. 1a). TCGA-CHOL cohort minimized the overexpressed genes from nine to seven, which included LAMA3, LAMA4, LAMA5, LAMB1, LAMB3, LAMC1 and LAMC2 (Fig. 1b), and analysis of the PCAWG data shared the six upregulated genes, except *LAMB1*, with the previous two datasets (Fig. 1c). Additionally, reprocessing of our previously collated microarray data revealed that out of 11, eight genes of laminin family, including LAMA1, LAMA2, LAMA3, LAMA5, LAMB1, LAMB3, LAMC2 and LAMC3 were significantly upregulated in CCA tissues when compared with the adjacent noncancerous tissues, and one gene, LAMA4, was downregulated (Fig. 1d). In sum, as demonstrated in Venn diagrams, LAMA3, LAMA5, LAMB3 and LAMC2 were the four genes which were concordantly overexpressed in four datasets (three RNA-seq and one microarray data) (Fig. 1e).

Validation of the expression of laminin genes in CCA tissues and cell lines

Here, we validated the upregulation of the four genes, namely LAMA3, LAMA5, LAMB3 and LAMC2, in 30 pairs of CCA and their matched adjacent noncancerous tissues as well as in CCA cell lines using real-time RT-PCR analysis. It is of note that LAMA3 has two transcript variants that are translated into proteins, LAMA3A and LAMA3B; nevertheless, only the truncated LAMA3 isoform is incorporated into the heterotrimeric laminins¹⁴. In tissues, the percentage of upregulated cases of the genes LAMA3A (29 cases; 97%), LAMA3B (17 cases; 56%), LAMA5 (19 cases; 66%), LAMB3 (24 cases; 80%) and LAMC2 (28 cases; 93%) outnumbered the combination of unchanged and downregulated cases (Fig. 2a). Mean FC of LAMA3B, LAMA5, LAMB3 and LAMC2 expression in CCA tissues compared to noncancerous counterpart were 3.5 (0.1–133 folds), 3.9 (0.3–216 folds), 9.2 (0.5–202

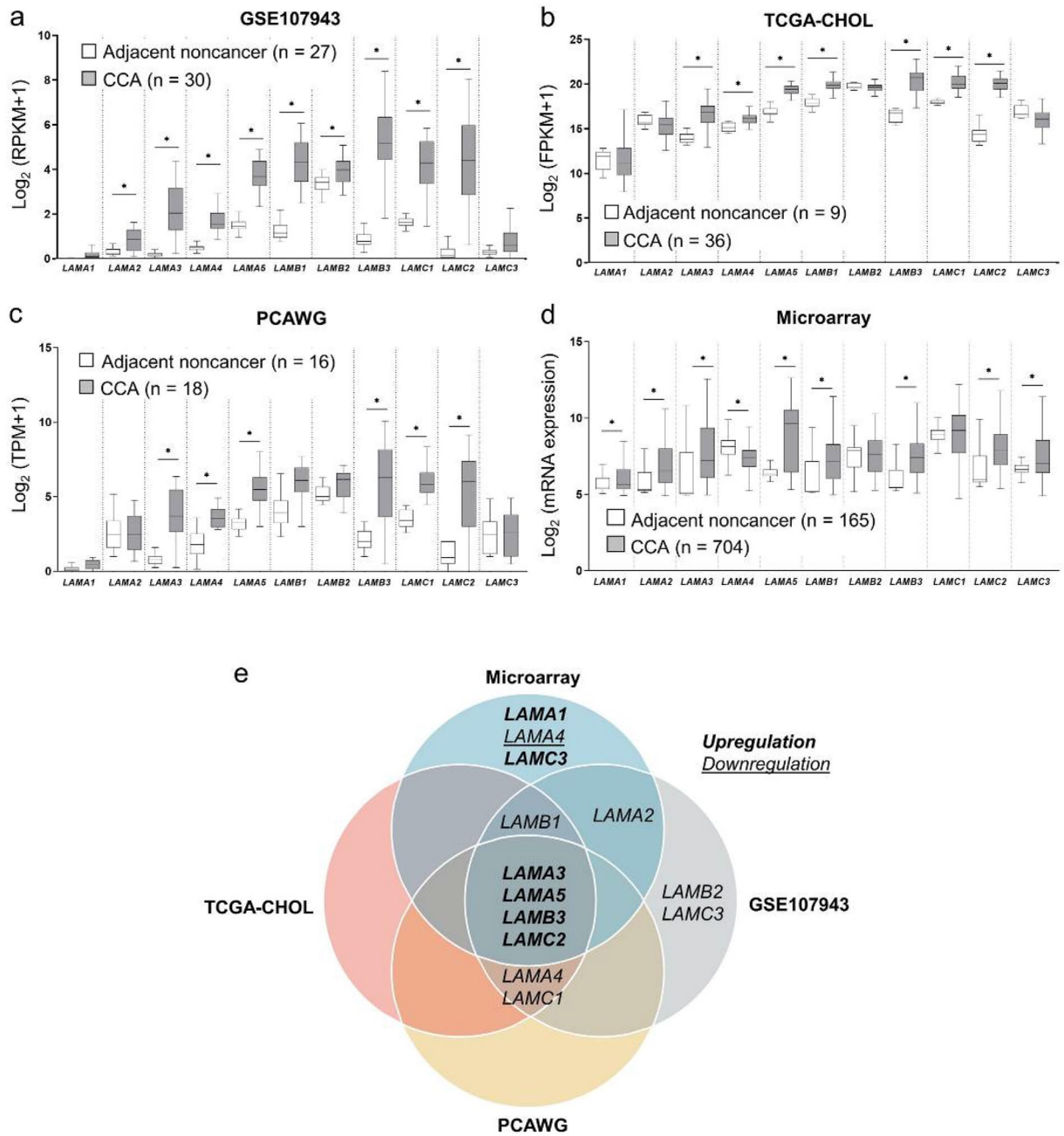


Figure 1. Gene expression profiling of laminin gene family in CCA through publicly available databases. Retrieved RNA-seq data from (a) GSE107943 dataset, (b) TCGA-CHOL cohorts and (c) PCAWG project, and (d) microarray data from ten integrated datasets. Graphs were created using Graphpad Prism. (e) Venn diagrams illustrating the common differentially upregulated genes in CCA shared by GSE107943, TCGA-CHOL, PCAWG and microarray. Statistically significant differences between groups were tested by Welch's t-test. * $P < 0.001$.

folds) and 37.7 (0.3–1,105 folds), respectively (Fig. 2b); however, there was no significant correlation between the expression levels and clinicopathology (Supplementary Table S1) as well as survival time of patients (Supplementary Fig. S1). Interestingly, LAMA3A relative expression was unable to be determined as its expression was too scarce to be detected in the majority of adjacent noncancerous tissues (27 out of 30) (Fig. 2b). The mRNA expression levels were further confirmed in CCA cell lines compared to immortal cholangiocytes MMNK-1. HuCCA-1 significantly showed the highest level of all four laminin genes, and the enhanced LAMA3A was also demonstrated in KKU-213. Although there was no statistically significant difference in KKU-213 expression in other genes, the trend towards upregulation were observed (Fig. 2c). In view of the above results, we conducted an examination of LAMA3 expression in paraffin-embedded tissues obtained from 50 CCA patients through immunohistochemical staining. Nevertheless, we observed LAMA3 presence in 37 cases (74%) of CCA tissues,

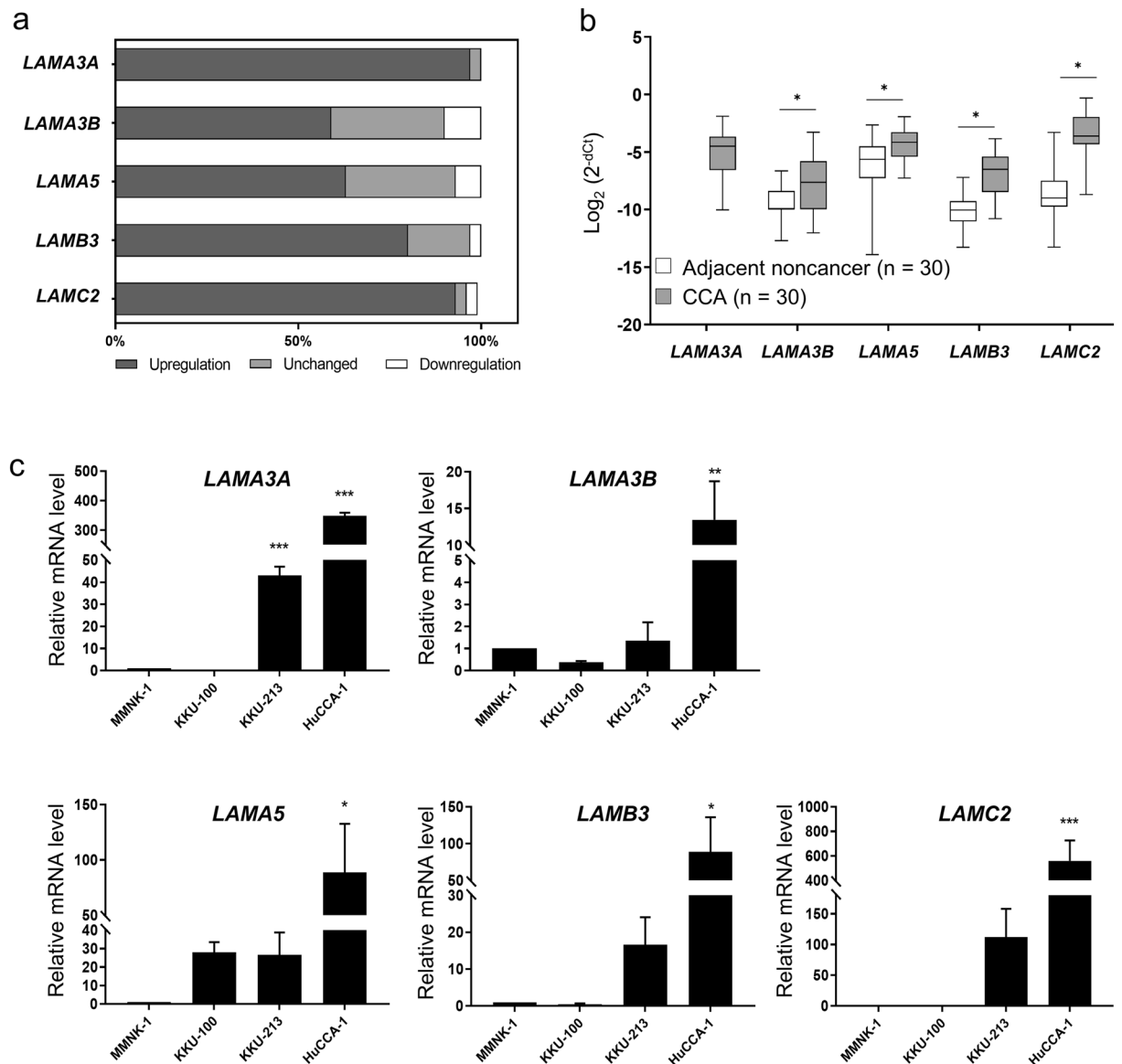


Figure 2. Validation of the expression of laminin genes in CCA tissues and cell lines using real-time RT-PCR. Relative mRNA levels of LAMA3A, LAMA3B, LAMA5, LAMB3 and LAMC2 in 30 pairs of CCA and their matched adjacent noncancerous tissues and in CCA cell lines were accessed using qPCR analysis normalized to *GAPDH*, and *18s rRNA*, respectively. (a) Percentage frequency of the cases with differential gene expression. Data were defined as upregulation and downregulation, according to $FC \geq 2$ and $FC \leq 0.5$, respectively. (b) The relative mRNA expression of CCA to their matched adjacent noncancerous tissues was evaluated using 2^{-dCt} formula and statistically analysed with Wilcoxon matched-pairs signed rank. (c) Relative mRNA levels of CCA cell lines to that of immortalized cholangiocyte MMNK-1 cells. Bar represents mean \pm SEM of three independent experiments. Figures were created using Graphpad Prism. * $P < 0.05$, ** $P < 0.01$, *** $P < 0.001$.

with its levels showing no significant correlation with either survival time or the clinicopathological aspects of the disease (Supplementary Fig. S2).

Association of high LAMA3 expression with focal adhesion pathway

Of all the datasets investigated, LAMA3, LAMA5, LAMB3 and LAMC2 were found to be commonly upregulated in cancer when compared to adjacent tissue samples as well as in CCA tissues and cell lines. Therefore, unsupervised hierarchical clustering analysis were performed using these four commonly upregulated genes which stratified the tumor tissue samples into high expression and low expression groups in all the cohorts (Fig. 3a–d). Further analysis to identify differential gene expression between the high and low expression groups in all the four different datasets investigated resulted in a total of 48 DEGs for GSE107943 dataset (Supplementary Table S2), 186 DEGs for the TCGA-CHOL (Supplementary Table S3), 482 DEGs for the PCAWG dataset (Supplementary Table S4) and 459 DEGs for the microarray datasets (Supplementary Table S5). The Venn diagram illustrating

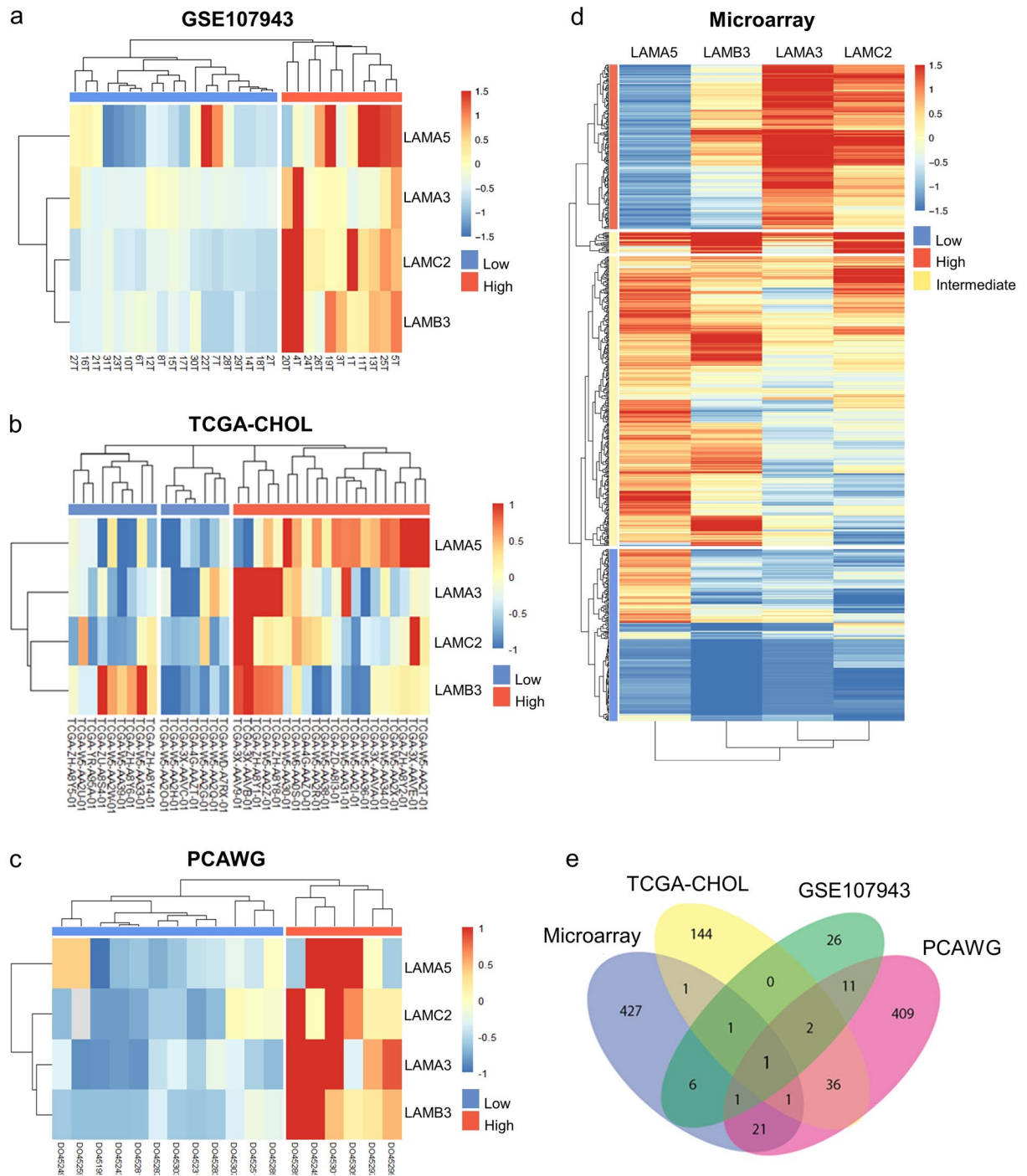


Figure 3. Identification of DEGs from hierarchal clustering analysis of laminin signature. Heatmap image of the four commonly upregulated laminin genes in (a) GSE107943, (b) TCGA-CHOL, (c) PCAWG and (d) microarray. (e) Venn diagram of DEGs listed from laminin signature in the four datasets. LAMA3 is the only DEG identified in all datasets. The DEGs screened based on $|\text{Log}_2\text{FC}| \geq 2$ with adjusted P -value < 0.05 . Figure were created using R Package.

the intersection of the DEGs revealed LAMA3 as the sole gene to be differentially expressed amongst these DEGs in all datasets investigated (Fig. 3e).

We further restratified CCA samples according to LAMA3 expression level as a means to elucidate biological pathways specifically associated with this gene (Fig. 4a). Using PCA, we identified that the sample clusters of microarray in the low and high group were prominently distinguishable, and therefore was selected for this analysis. Transcriptomic changes and pathways affected were investigated (Fig. 4b). The result showed that 198 DEGs were found; with 155 upregulated and 43 downregulated as represented in the heatmap and the volcano

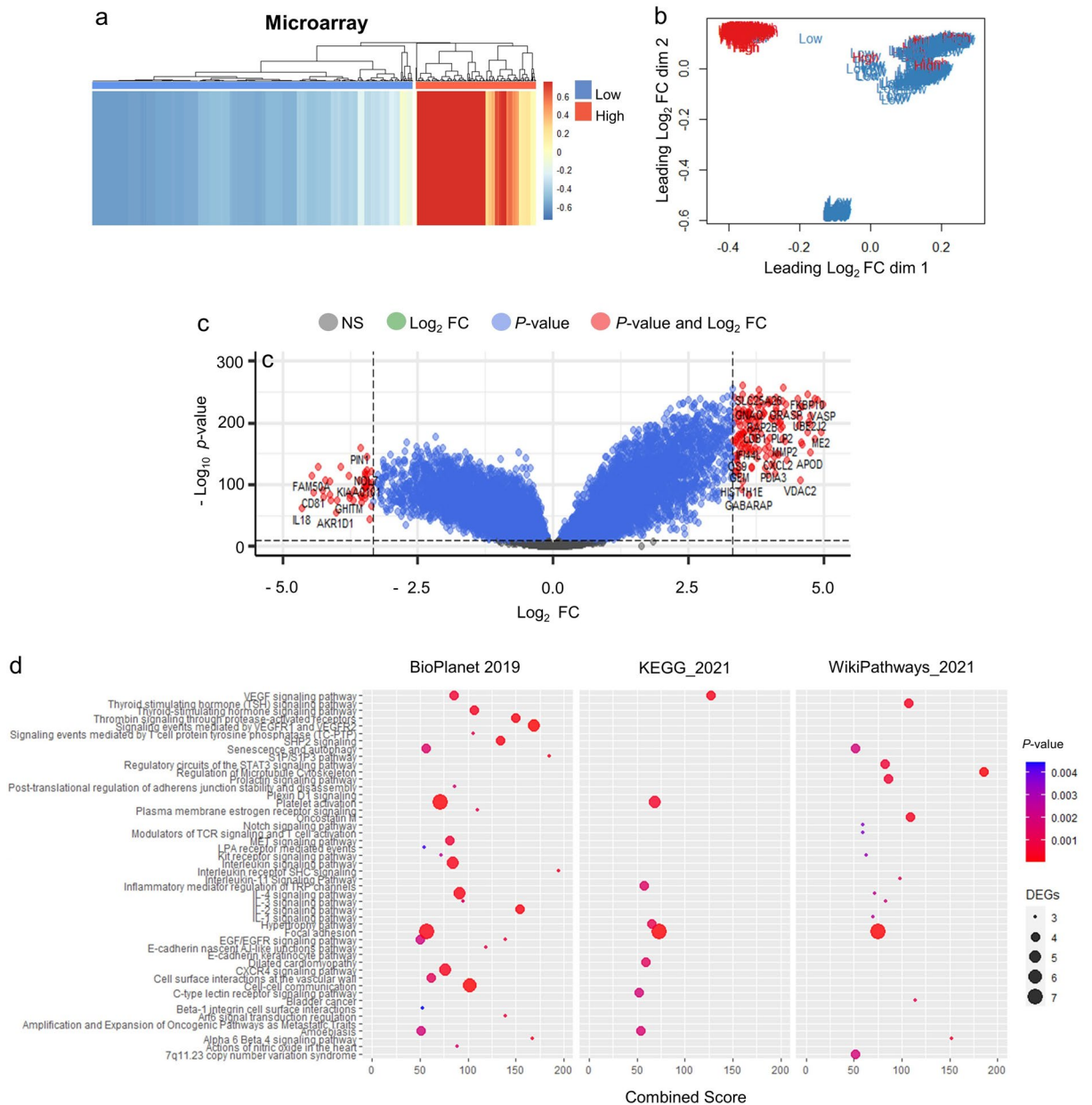


Figure 4. The DEGs and pathway enrichment analysis acquired unsupervised hierarchical clustering of LAMA3 stratified CCA sample of microarray dataset. **(a)** Heatmap image and **(b)** PCA plot indicating the separation low and high LAMA3 expression. **(c)** DEGs in high vs low LAMA3 expression group. Statistically significant DEGs cut-off are with the adjusted $P < 0.05$ and the $\text{Log}_2 \text{FC}$ of 3.32. **(d)** Pathway enrichment analysis of DEGs using EnrichR consolidated databases: BioPlanet, KEGG and Wikipathways. DEGs were considered at $\text{FC} > 2$ and $P < 0.05$. Enriched pathway were considered when combined score > 50 .

plot (Fig. 4c and Supplementary Table S6), and these DEGs were concordantly enriched for ‘focal adhesion’ in three pathway databases consolidated in EnrichR, including BioPlanet, KEGG (Kyoto Encyclopedia of Genes and Genomes) and WikiPathways (Fig. 4d and Supplementary Table S7). The DEGs involved in focal adhesion pathways were upregulated, which included *ITGA7*, *PIK3R1*, *PPP1R12A*, *SRC*, *VASP* and *VEGFA*. The expression of some of these genes was explored in LAMA3 silencing KKKU-213 using real time RT-PCR and we observed the statistically significantly decreased in *SRC* expression, but not in *ITGA7*, *PIK3R1* and *VASP* (Supplementary Fig. S3). Interestingly, several cancer progression-associated pathways, such as interleukin signalling, cell–cell communication and microtubule cytoskeleton regulation were enriched, suggesting the importance of LAMA3 in CCA malignancy (Fig. 4d). Together these results highlight the unique importance of LAMA3 in the laminin family in CCA.

Effects of LAMA3 silencing on CCA cell proliferation, cell death and cell cycle progression

Having recognized the significance of LAMA3 across the four datasets, the biological roles of LAMA3 on the progressive phenotypes of CCA were evaluated by the transient knockdown using siRNA targeting LAMA3 mRNA (siLAMA3). Compared with siNeg transfection, the siLAMA3 treatment effectively inhibited basal LAMA3A mRNA expression level of HuCCA-1 and K KU-213 by 73% and 86%, respectively (Fig. 5a), but barely affected expression of LAMA3B variant (Supplementary Fig. S4). In proliferation assay, cells were allowed to proliferate for 72 h before MTS assay. The data demonstrated that LAMA3 knocking down significantly reduced cell proliferation of both cell lines, substantially in K KU-213 with 55% decrease (Fig. 5b). To further understand the inhibitory effect of LAMA3 suppression on cell proliferation, we performed flow cytometry to investigate the induction of cell death and the distribution of specific phases of cell cycle. The results showed that suppression of LAMA3 did not affect cell death in both cell lines (Fig. 5c), but induced the G0/G1-phase arrest, resulting in the decreasing trend in S and G2/M phase entry of the cell cycle in K KU-213, compared with the control cells (Fig. 5d).

Reduction of CCA cell adhesion and migration

Cell adhesion and cell migration are the critical steps in the invasive process of metastatic tumor cells, we assessed whether LAMA3 silencing dysregulated the adhesive and motility abilities of CCA cells. Forty-eight-hour-post transfected HuCCA-1 and K KU-213 cells were seeded and allowed to adhere on plate for 6 and 12 h, respectively, prior to the removal of non-adhered cells. Disrupting LAMA3 expression by siLAMA3 reduced adhesive ability of both CCA cells with only $36.0 \pm 10.4\%$ and $26.7 \pm 9.7\%$ of LAMA3-silenced HuCCA-1 and K KU-213 cells remained attached to the plate compared to the siNeg control (Fig. 6a); furthermore, LAMA3-silenced cells formed smaller cell spreading area as shown in the inserts of Fig. 6a. In addition, precoating of mock-derived decellularized ECM on the plate was able to restore the adhesive ability and the spreading area of both LAMA3-silenced cells to the comparable levels as those of the siNeg control cells (Fig. 6a). Tracking of the individual migrating cells using time-lapse video microscopy revealed that migration speed of LAMA3-silenced K KU-213 cells ($10.1 \pm 0.2 \mu\text{m/hr}$) was significantly slower compared to that of the siNeg control cells ($15.6 \pm 0.2 \mu\text{m/hr}$); however, the migration speed of LAMA3-silenced HuCCA-1 cells remained unchanged (Fig. 6b) (Supplementary Video S1 and S2). Therefore, we utilized in vitro transwell migration assay to investigate cell migration and found that in response to knocking-down of LAMA3, cell motility of HuCCA-1 and K KU-213 was declined by 93% and 86%, respectively, compared to that of siNeg treated cells (Fig. 6c), indicating the propensity roles of LAMA3 in promoting cell adhesion and migration.

EMT status and cell morphology of LAMA3-silenced cells

Activation of focal adhesion kinase (FAK) through autophosphorylation at Tyr397 is involved in regulating EMT-mediated cancer progression and affects the expression of EMT-related proteins¹⁵. Hence, we determined the pFAK/tFAK ratio and the EMT status following LAMA3 knockdown, and it exhibited that inhibition of LAMA3 significantly decreased this ratio and suppressed the expression of the EMT-inducing transcription factor Slug, vimentin and claudin-1 but not significantly affected E-cadherin expression when compared with siNeg cells (Fig. 7, Supplementary Fig. S5). However, immunofluorescence staining demonstrated a significant increase in the localization of E-cadherin to the cell membrane in both CCA cells and particularly pronounced in the K KU-M213 cells after LAMA3 knockdown (Fig. 8a,b). Furthermore, phalloidin staining confirmed a reduction in cell spreading area by 27.8% and 56.2% in LAMA3-silenced HuCCA-1 and LAMA3-silenced K KU-213 cells, respectively, compared to siNeg-treated cells (Fig. 8c). Consistent with the decrease in cell spreading, we observed a significant increase in the circularity (close to one) of the HuCCA-1 cells after LAMA3 silencing (Fig. 8d). However, due to the drastic loss in adhesive property of LAMA3-silenced K KU-213 cells, there were not enough single cells for measuring the circularity. Collectively, we clarified that LAMA3 knockdown could inhibit proliferation, adhesion and migration; induce the G0/G1-phase arrest; and regulate EMT in CCA cells.

Discussion

Extensive literature has indicated that the aberrantly increased deposition of matrix proteins in CCA TME contributes to the enhanced malignant behaviors of the disease¹⁶. Hence, the better understanding of the associations between TME and the aggressiveness of CCA may be critical to improve the prognosis and therapy of CCA patients. We previously revealed that the exogenous laminin was the most potent inducer for CCA migration and adhesion¹⁰; however, the roles of endogenous laminins pertaining to CCA progression remain poorly understood. Here, bioinformatics analysis identified LAMA3, LAMA5, LAMB3, and LAMC2 as the commonly upregulated laminin subtypes in CCA and the unique overexpression of LAMA3 transcript was confirmed in Thai CCA patient tissues and cell lines. Furthermore, silencing of the candidate laminin subtype LAMA3 diminished CCA cell proliferation, adhesion and migration, together with reversing EMT progress.

The availability of huge amounts of transcriptome data has upgraded the knowledge in the cancer research field. The present meta-analysis selected the datasets based on the variety of transcriptomic techniques and ethnic heterogeneity, thus increasing the sample size and the reliability of results and averting the difference of patients' background. This may allow the development of more precise targeted strategies. In concordance with in silico analysis, real time RT-PCR validated the upregulation of LAMA3, LAMA5, LAMB3 and LAMC2 in Thai CCA cell lines and patient tissues in which LAMA3A was upregulated the most and in nearly all cases (29 out of 30), pointing out the potentiality to use LAMA3 detection as the diagnostic approach to distinguish CCA patients from normal cases. However, there was no correlation between the expression levels with clinicopathology and overall survival. This discrepancy might be clarified through large-scale clinical studies.

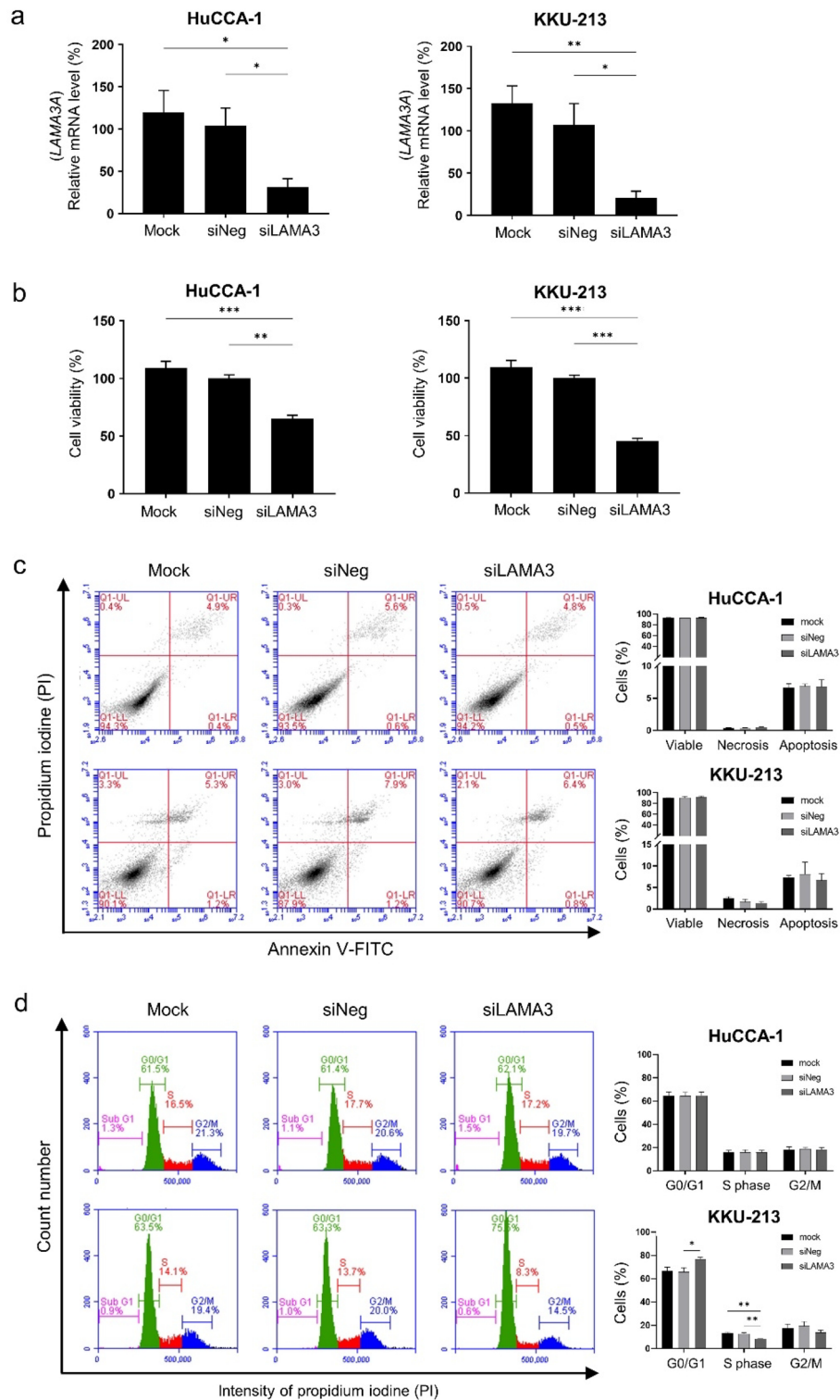


Figure 5. Effects of LAMA3 knockdown on CCA cell proliferation, cell death and cell cycle progression. **(a)** Efficiency of siLAMA3 on the reduction of LAMA3A expression in CCA compared with those of siNeg treatment at 48 h-post transfection. **(b)** Cell proliferation of CCA cell transfected with siLAMA3 determining at 72 h-post transfection using MTS assay. **(c)** Representative area histograms and quantified bar graph for the distribution of cell cycle phases. Data present as mean \pm SEM of siLAMA3 relative to siNeg from three independent experiments. Graphs were created using Graphpad Prism. Scatter plots and area histograms of flow cytometry were generated from The BD Accuri™ C6 Plus Flow Cytometer. * $P < 0.05$, ** $P < 0.01$, *** $P < 0.001$.

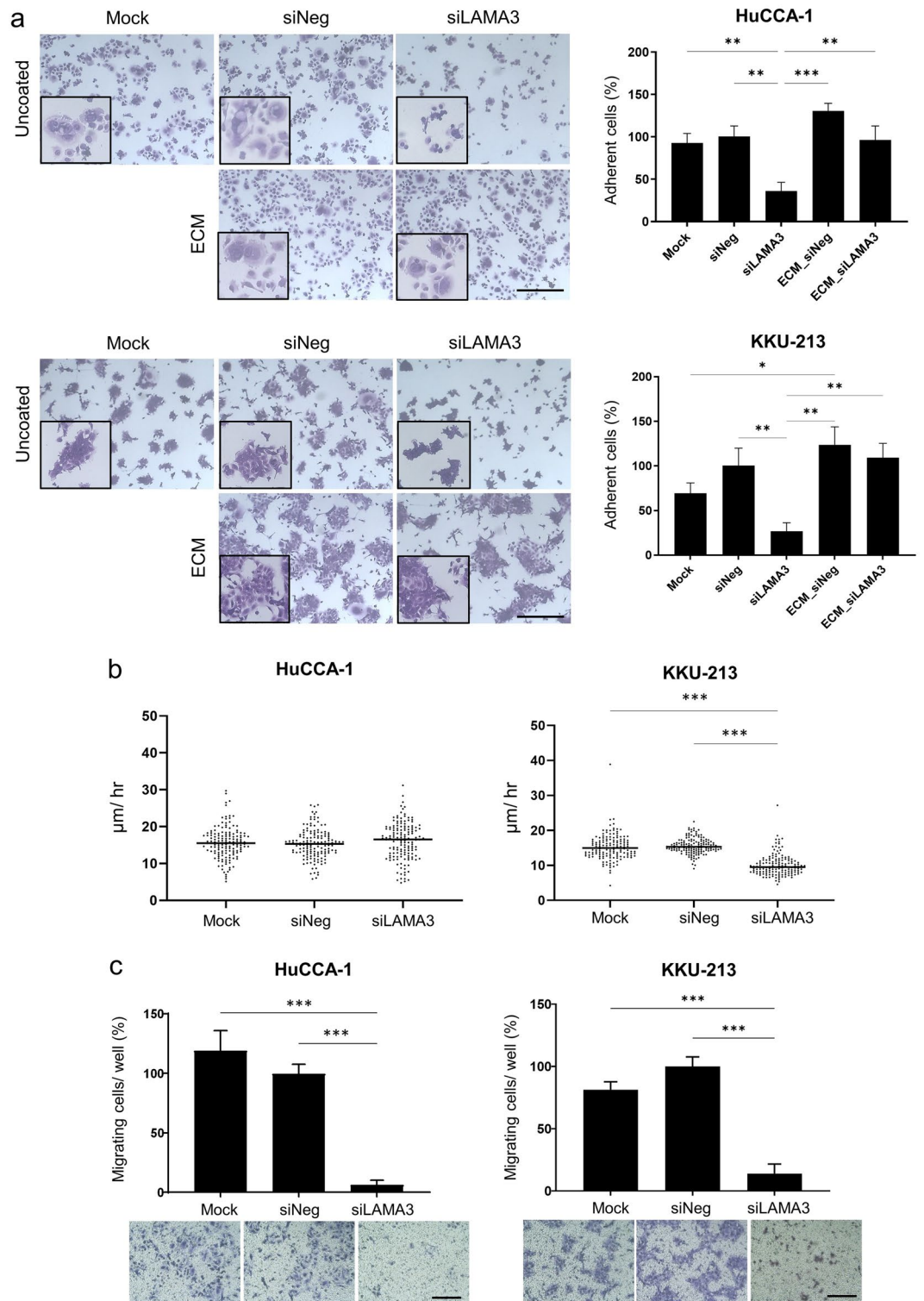


Figure 6. Reduction of CCA cell adhesion and migration in LAMA3-silenced cells. **(a)** Cell adherent area analyzed by Image J (right). Data present as mean \pm SEM in percent relative to those of the siNeg from three independent experiments. Representative crystal violet staining of adherent cells under 10 \times magnification and the inserts represent enlarge areas (left). Scale bar: 40 μ m. ECM: mock-decellularized ECM-coated plate. **(b)** Migration speed of CCA cells collected by cell tracking in time-lapse every 15 min for 12 h. Data from one representative experiment were shown in dot plots, in which individual dots represent the average migration speed (μ m/hour) per area (n = 150). **(c)** Cell migration examined by the transwell assay. Graphs were created using Graphpad Prism. * $P < 0.05$, ** $P < 0.01$, *** $P < 0.001$.

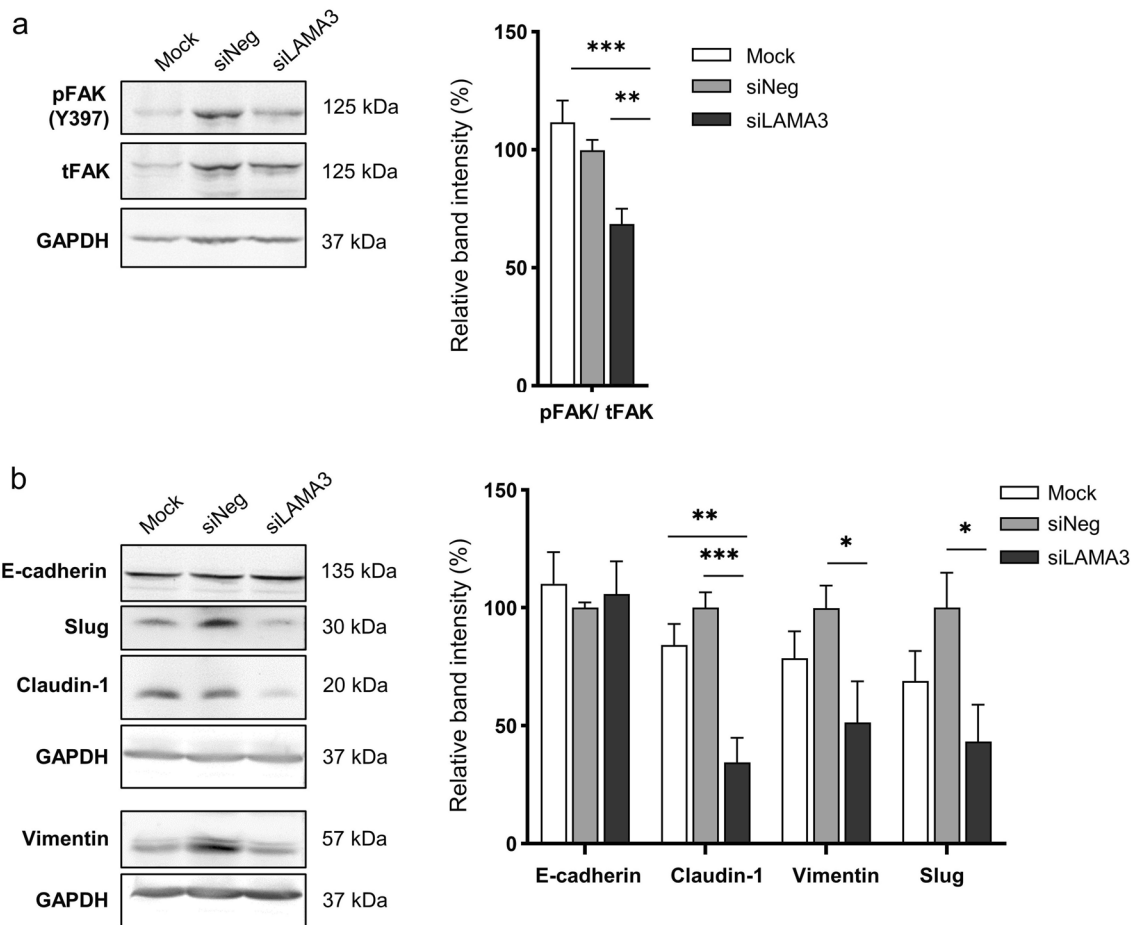


Figure 7. Representative western blotting illustrated the decrease in the pFAK/tFAK ratio and the inhibition of EMT markers expression in KKU-213 cells transfected with LAMA3 siRNA. Treated cells were reseeded for 24 h before protein extraction and GAPDH was used as the internal control. The cropped blots are used in the figure. The membranes were cut prior to exposure so that only the portion of gel containing the desired bands would be visualized. Full-length blots are presented in Supplementary Fig. S4. **(a)** Expression of FAK and its phosphorylation at Y397. **(b)** Expression of EMT-markers, including vimentin and Slug, and the epithelial markers, E-cadherin and claudin-1. Band intensity was shown as mean \pm SEM in percent relative to those of the siNeg from at least four independent experiments. Graphs were created using Graphpad Prism. * $P < 0.05$, ** $P < 0.01$, *** $P < 0.001$.

The four upregulated laminin subtypes have been previously reported of their tumorigenic effects. LAMA5 is primarily important for the proliferation induction in cancer cells¹⁷ and also upregulated in CCA-associated fibroblasts¹⁸. LAMB3 is involved in invasive and metastatic behaviors of various cancers, especially pancreatic adenocarcinoma (PAAD) by modulating the PI3K (phosphoinositide 3-kinases)/ Akt signaling pathway¹⁹. The product of this gene was also distinctively detected in the secretome of HuCCA-1, but not that of hepatocarcinoma cell lines²⁰. An aberrant overexpression of LAMC2 was usually associated with worse prognosis for patients with bile duct, bladder, colon and lung cancers¹⁴. In CCA, Pei Y. et al. demonstrated the link of highly expressed LAMC2 to the activation of the epidermal growth factor receptor (EGFR) signaling pathway and EMT which leads to cell invasion, migration and angiogenesis²¹. Unlike other dysregulated laminins, expression level and roles of LAMA3 across different tumors are paradoxical. Using GEPIA2 analysis, we here revealed that LAMA3 was upregulated in various types of cancers such as colon, kidney, liver, pancreas and rectum, but downregulated in some cancers, viz. breast, lung and skin (Supplementary Fig. S6)²². Highly expressed LAMA3A splice variant in head and neck squamous cell carcinoma is strongly associated with poor survival outcome²³. On the other hand, loss of LAMA3 induces cell invasion and macrophage infiltration in cutaneous squamous cell carcinoma²⁴.

To identify gene expression pattern related to laminin expression signature, CCA tumors in each transcriptomic dataset were classified into low and high expression using hierarchical clustering analysis. Surprisingly, the analysis demonstrated that LAMA3 was the only DEG overlapped in all four datasets investigated. Further re-stratifying the tumor samples according to LAMA3 expression level could enrich the 'focal adhesion' in multiple pathway databases; however, in this part the enrichment pathway analysis was exclusively performed in microarray datasets owing to the clear separation between low and high populations (Fig. 4d, Supplementary Fig. S7). Focal adhesions are formed at the cell-ECM contact points to initiate signalling events important for a variety of biological processes like cell motility, cell proliferation, cell differentiation, regulation of gene expression

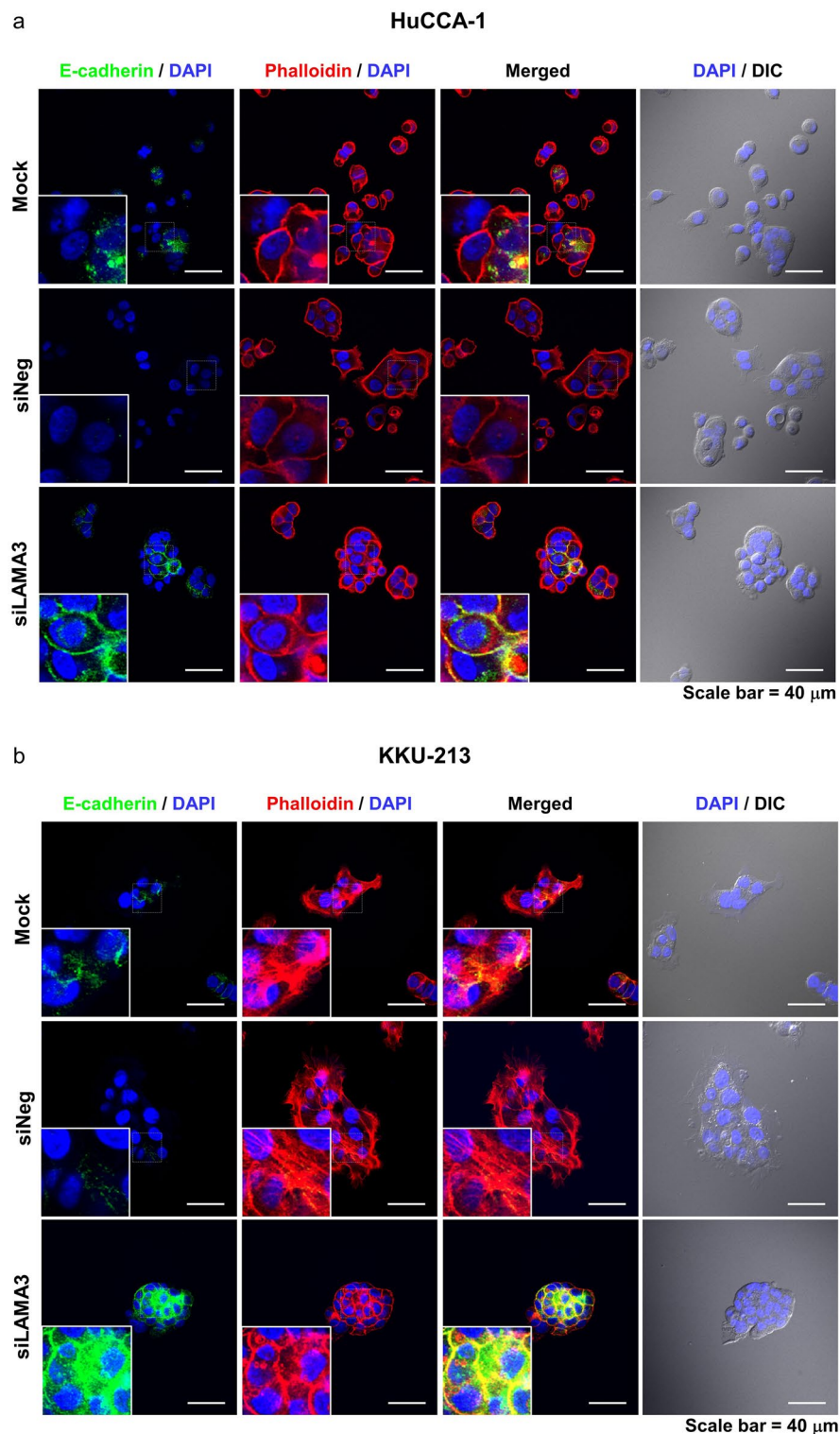


Figure 8. Alteration of E-cadherin and F-actin distribution and shrinkage of cell spreading area in CCA cells upon LAMA3 knockdown. Forty-eight-hr LAMA3-silenced cells were reseeded for 24 h before immunofluorescent staining. **(a,b)** Immunofluorescent images showed localization and distribution of E-cadherin protein (green), F-actin (using phalloidin staining, red), and nuclei (Hoechst staining, blue). **(a)** HuCCA-1; **(b)** KKU-213; scale bar: 40 μ m. **(c)** The cell size in the unit area ($\mu\text{m}^2/\text{cell}$) and **(d)** cell circularity was measured from phalloidin staining. Data from one representative experiment were shown in box plots. The value close to one indicates high circularity. (cell spreading: $n > 40$, circularity = $n > 15$). Images were captured from FV1000. ****** $P < 0.01$, ******* $P < 0.001$.

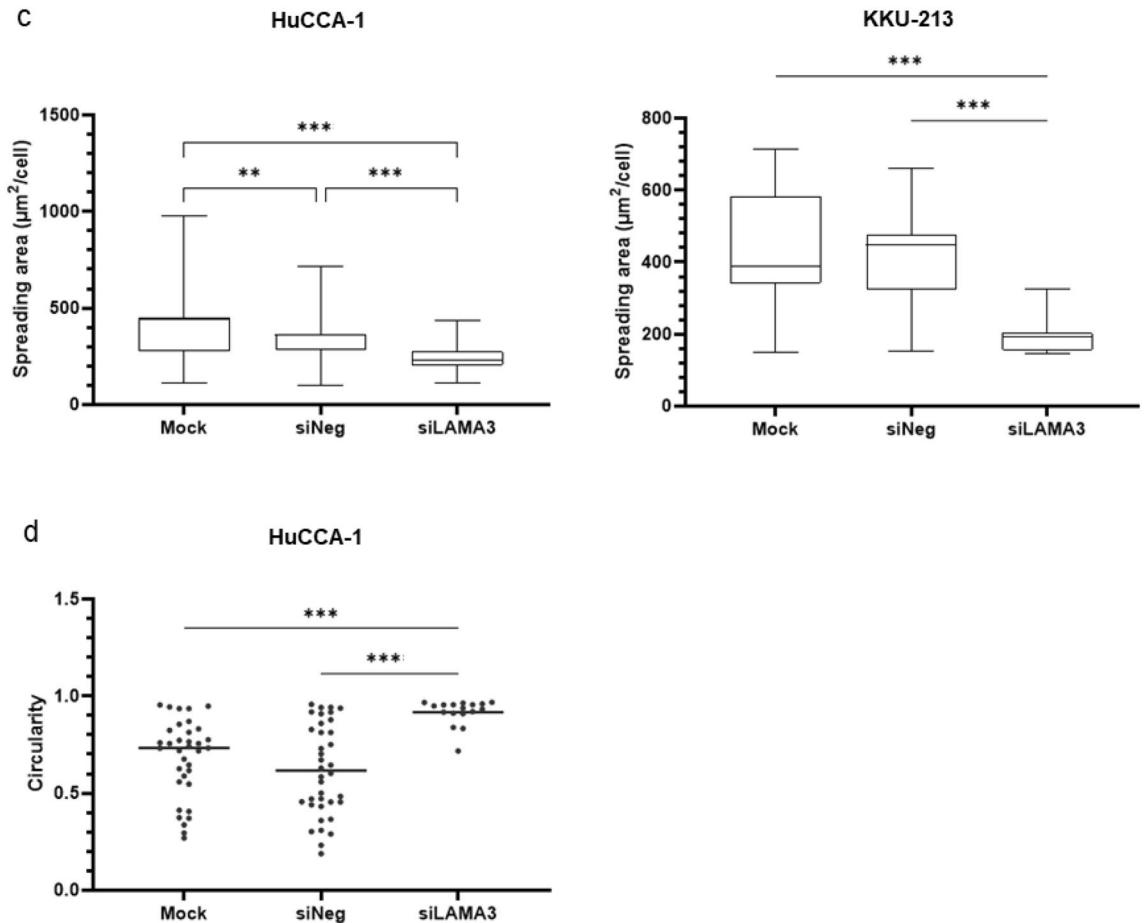


Figure 8. (continued)

and cell survival⁷. Interestingly, several cancer progression-associated pathways, such as interleukin signalling, cell–cell communication and microtubule cytoskeleton regulation were also enriched, suggesting the importance of LAMA3 in CCA malignancy. As the $\alpha 3$ chain generally harbors the binding sites for its cognate receptors and its importance has not been well understood in CCA²⁵, these rationalized the functional investigation for LAMA3 on CCA progression.

In the current work, the roles of LAMA3 in CCA malignancy were investigated using two high LAMA3 expressing CCA cell lines, KKKU-213 and HuCCA-1, established from Thai patients with intrahepatic CCA. Our findings demonstrated that LAMA3 knockdown hindered cell proliferation, adhesion and migration and EMT induction as shown by decreased expression of vimentin and Slug. The EMT-transducing transcription factor Slug activates vimentin expression and in turn represses E-cadherin⁸. However, we revealed that the reduction of Slug did not disturb E-cadherin expression and this result is in line with Huang’s work showing that silencing LAMA3 expression decreases vimentin but has no effect on E-cadherin expression in PAAD cell lines named PANC-1²⁶. Claudin-1 has bifunctional roles: maintaining epithelial cell polarity and facilitating collective migration²⁷. We found that silencing LAMA3 downregulated claudin-1 expression, suggesting its role in inducing collective migration in KKKU-213 as observed in Supplementary Video S2.

Although the knockdown efficiency of siLAMA3 treatment was relatively close in the two cell lines, some LAMA3 silencing effects were remarkably different. For example, LAMA3 knockdown reduced migration speed of KKKU-213 detected by time-lapse imaging, yet it did not affect those of HuCCA-1. Moreover, it decreased proliferation of KKKU-213 (55%) more than that of HuCCA-1 (35%). These might account for several contributing factors. The most likely cause is that HuCCA-1 has a significant higher level of basal LAMA3 mRNA so large amount of the predeposited LAMA3 secreted prior to knockdown (Supplementary Fig. S8) might play role in maintaining migration speed of LAMA3-silenced HuCCA-1. Consequently, we could observe the reduction in cell migration using transwell migration assay in which the cells were reseeded after knockdown, thus eliminating the LAMA3 predeposited effect. Secondly, their $\alpha 3$ chain may undergo different proteolytic post-translational modifications; for example, HuCCA-1, but not KKKU-213, abundantly secretes plasminogen activator inhibitor type 1 (PAI-1), major inhibitor of plasminogen activator/plasmin system²⁸. Finally, they might distinctively transduce intracellular signalling due to the difference in laminins’ cognate receptors; for instance, HuCCA-1 prominently expresses $\beta 4$ integrin and its cooperative partner c-Met, while KKKU-213 remarkably produces 36/67 kDa laminin receptor and ErbB2^{10,29–32}.

The findings of this study have to be seen in light of some limitations. First, because not all the datasets we utilized in the current study provide histological information, our *in silico* results generalize the biological effects of LAMA3 in both intrahepatic CCA and extrahepatic CCA. Future research can investigate its connection with specific histological types of CCA. Second, we still have inadequate information about the clinicopathological data and demographic variables of the biological samples used in the *in silico* analysis. Third, it is worth noting that the number of matched paired-tissue samples from the same donors may yield a reliable result as paired-sample RNA-seq significantly enhances not only the sensitivity in the detection of differential expression but also the statistical power³³, thus further research could be carried out to explore this point. Last but not least, our results should be carefully interpreted and applied due to the resemblance to PAAD in the abundance of ECM proteins, like LAMA3, LAMB3 and LAMC2^{26,34,35}.

To our knowledge, this is the first report to reveal the expression signature of laminin gene family in CCA and the impacts of LAMA3 on promoting CCA cell proliferation, adhesion and migration. The analysis undertaken here has broadened the understanding of CCA TME and emphasizes the need to expand preclinical studies with appropriate animal models more closely mimicking CCA TME that would accurately predict stromal interaction with CCA cells. In addition, our findings suggest that LAMA3 may be the promising diagnostic marker and therapeutic target to overcome the desmoplastic nature of CCA.

Materials and methods

Clinical tissue specimens and cell culture

A total of 30 pairs of frozen CCA and matched adjacent noncancerous tissues were obtained from patients who had undergone hepatic resection at Srinagarind Hospital, Khon Kaen University, Thailand and the tissue specimens were confirmed for CCA by the pathologist. The study protocol was approved by The Human Research Ethics Committee, Khon Kaen University (HE571283) and exempted by Mahidol University Central Institutional Review Board (MU-CIRB 2019/098.2803). All methods were carried out in accordance with the World Medical Association Declaration of Helsinki and informed consent was obtained from all patients or legally authorized representatives included in the study.

Thai patient-derived CCA cell lines, KKU-100 (RRID:CVCL_3996)³⁶ and KKU-213³⁷ as well as the immortalized cholangiocyte cell line MMNK-1 (RRID:CVCL_M266)³⁸ were purchased from the Japanese Collection of Research Cell Bank (JCRB), and the intrahepatic CCA cell line HuCCA-1³⁹ was generously provided by Professor Sititaya Sirisinha (Mahidol University, Bangkok, Thailand). Cell lines were cultured in HAM's F-12 medium supplemented with 15 mM HEPES, 14 mM NaHCO₃, 1% antibiotic-antimycotic solution (penicillin, streptomycin and amphotericin B) and 10% heat-inactivated fetal bovine serum (GIBCO) in a humidified incubator at 37°C with 5% CO₂.

Gene expression profiling of laminin gene family analyzed from public transcriptome databases

Baseline mRNA expression of laminin gene family (11 genes)—namely LAMA1-5, LAMB1-3 and LAMC1-3—in CCA tumor and adjacent noncancerous tissues was analyzed in three independent RNA-seq datasets, including GSE107943, The Cancer Genome Atlas (TCGA)⁴⁰ and The International Cancer Genome project: Pan-Cancer Analysis of Whole Genomes (PCAWG; <https://docs.icgc.org/pcawg>)⁴¹. First, the RPKM (reads per kilobase of transcript per million reads mapped) data of GSE107943 dataset, containing 30 CCA samples with 27 matched normal liver tissues, was retrieved from GEO (www.ncbi.nlm.nih.gov/geo/), using the search terms "cholangiocarcinoma" AND "human" AND "RNA-seq". Second, the FKPM (fragments per kilobase of transcript per million reads mapped) data from TCGA-CHOL cohort containing 36 CCA tumor and nine match TCGA normal samples was obtained from cBioportal (www.cbioportal.org). Third, the TPM (transcript per million) data from PCAWG project was acquired from the ArrayExpress (www.ebi.ac.uk) using the accession number "E-MTAB-5423" which contained 18 tumor tissues and 16 noncancerous adjacent tissues.

The transcriptomic profiles were further explored based on our previously collated microarray data obtaining from 10 independent cohorts (GSE132305, GSE2263, GSE26566, GSE32225, GSE32879, GSE35306, GSE5755, GSE66255, GSE76297 and GSE89749) from GEO database, which included 704 CCA tumor and 165 adjacent noncancerous tissues⁴². The combined datasets were undergone Log₂(x + 1) transformation, where "x" is signal intensity. The differential expression of specified genes in CCA tumors and noncancerous tissues was compared using Welch's *t*-test. *p*-value < 0.001 was considered differentially expressed genes.

RNA isolation and quantitative real-time PCR (qRT-PCR)

RNA was extracted from liver tissues of CCA patients by coarsely homogenizing the tissue in TRIzol™ Reagent (Invitrogen) as previously described⁴³. The RNA concentration and quality (260/280 ratio) were determined using a Nano Drop UV-spectrophotometer (Thermo Fisher Scientific). The RNA (2 μg) was reversely transcribed into cDNA employing random hexamer primers and HyperScript™ RT—Master mix (GeneAll Biotechnology). Real-time PCR analysis was performed in a 10-μl mixture containing cDNA (25 ng), 1X FastStart Universal SYBR Green Master cocktail (Roche Diagnostics) and specific primer pair (0.5 μM of each) using the CFX96 Touch System (Bio-Rad) under the following thermocycling reactions: 95 °C for 5 min; 40 cycles of 94 °C for 45 s; 55 °C for 30 s; and 72 °C for 30 s. The primers sequences were listed as follows: 18srRNA (5'-CCATCCAATCGG TAGTAGCG-3', 5'-GTAACCCGTTGAACCCATT-3'), GAPDH (5'-CACCAGGGCTGCTTTAACTCTGG-3', 5'-CCTTGACGGTGCCATGGAATTTGC-3'), LAMA3A (5'-GTTCACAGCAGCAAAGGGTG-3', 5'-CAATTG CAGGAACACACCG-3'), LAMA3B (5'-TAGACTTTGGAAGCACCTACTCA-3', 5'-GTTTATCAAGGACAC CACAACCT-3'), LAMA5 (5'-TGCATCGAGATGGACAGC-3', 5'-GCTTCAGGAAGAAGAGCA-3'), LAMB3 (5'-GGCTGCGACAAGGCATCA-3', 5'-CACCG GGTAGCGATTACAGTA-3'), LAMC2 (5'-CCAGGAGGG

AAGTCTGTGATT-3', 5'-TCTGTGCCGGTAAAAGCC AT-3'). Gene expression was quantified relative to the internal control gene GAPDH using the $2^{-\Delta\Delta Ct}$ method⁴⁴. Fold-change (FC) for gene expression in CCA compared to matched adjacent noncancerous was calculated with the $2^{-\Delta\Delta Ct}$ method, which defined $\text{Log}_2 \text{FC} > 1$ as upregulation and < -1 as downregulation.

The RNA of cell lines (70–80% confluence) was extracted using a Blood/Cell Total RNA Mini Kit (Geneaid) following the manufacturer's instruction. Relative mRNA levels of CCA cell lines to those of immortalized cholangiocyte MMNK-1 cells were quantified by $2^{-\Delta\Delta Ct}$ method using 18S rRNA for normalization⁴⁴. Three independent experiments were performed, each with triplicate assays.

Differential gene expression analysis

Unsupervised hierarchical clustering was conducted to explore whether the filtered gene signature expression can be used to stratify CCA patients. Heatmap was drawn using the pheatmap package. Samples were then grouped according to the clusters corresponding to the low- and high-expression of the commonly upregulated laminin genes across all datasets. To assess the differences in transcriptomic profiles between samples with low and high expression of the filtered gene list, Principal Component Analysis (PCA) and differential gene expression analyses were conducted using the DESeq2 package (RRID:SCR_015687) for the RNA-seq datasets and limma package (RRID:SCR_010943) for the Microarray datasets in R version 4.0.2. *P*-values were determined by Wald statistics and an adjusted *P*-value (*Q*-value) to correct for multiple comparisons testing using the Benjamini–Hochberg method. DEGs were defined as genes with $2 \times \text{FC}$ for GSE107943, TCGA-CHOL, PCAWG and $10 \times \text{FC}$ for the microarray datasets with adjusted *P*-value < 0.05 . Results were visualized using 'Enhanced Volcano' (RRID:SCR_018931) and 'ggplot2' (RRID:SCR_014601) packages. This analysis was also repeated using a re-stratification with just LAMA3 alone. Differentially expressed genes were then analyzed in iLincs SPIA analysis (www.ilincs.org; Accessed online on August 1st, 2022) using using EnrichR consolidated pathway analysis databases (<https://maayanlab.cloud/Enrichr/>; Accessed online on August 1st, 2022)^{45–47}, namely BioPlanet, KEGG⁴⁸ and WikiPathways for signaling pathway enrichment, which was sorted with DEGs $> 2\text{-FC}$, combined score > 50 and *P*-value < 0.05 .

Silencing of LAMA3 expression

Small interfering RNAs (siRNAs) were transfected into CCA cell lines using Lipofectamin RNAiMAX reagent (Thermo Fisher Scientific), according to the manufacturer's instruction. Cells were seeded in a six-well plate at the density of 1.5×10^5 cells/ well (HuCCA-1) and 2×10^5 cells/ well (KKU-213), or in a 96-well plate at the density of 3,000 cells/ well (HuCCA-1) and 4,000 cells/ well (KKU-213) for 24 h prior to transfection with 15 nM siRNA targeting LAMA3 (siLAMA3) (sc-35789; Santa Cruz Biotechnology). AllStars Negative Control siRNA (1027280; Qiagen) was used as control (siNeg). Transfecting medium was replaced with fresh complete media at 24-h post-incubation. Forty-eight hour-post transfection, efficiency of siLAMA3 was evaluated using qRT-PCR and protein expression profile and cell biological phenotypes were assayed as described below.

MTS assay

The effect of LAMA3 depletion on cell proliferation was examined using the MTS assay. After transfection, the cells were allowed to proliferate for 72 h prior to addition of MTS reagent (3-(4,5-dimethylthiazol-2-yl)-5-(3-carboxymethoxyphenyl)-2-(4-sulfophenyl)-2H-tetrazolium) (ab197010; Abcam) to each well and further incubation for four hours according to the manufacturer's instructions. The absorbance at 490 nm was recorded using Multiskan Skyhigh Microplate Spectrophotometer (Thermo Fisher Scientific). The data were collected from three independent experiments each done in triplicate.

Cell adhesion assay

After forty-eight hours of transfection, HuCCA-1 (1×10^4 cells) and KKU-213 (1.5×10^4 cells) in 100 μl were seeded in 96-well plates and incubated for 6 and 12 h, respectively. Non-adherent cells were removed. Adherent cells were washed twice with cold PBS, fixed with cold absolute methanol for 15 min, stained with 0.5% crystal violet for 10 min, washed with tap water and air-dried. Images were captured in four random fields under $4 \times$ magnification and cell-adhesive area was measured using Image J 1.52h (RRID:SCR_003070). The mean adhesion area of siNeg from three independent experiments was set as the reference (100%), and the adhesion area for each experimental condition was calculated as a percentage relative to the siNeg mean. These percentages were then plotted as the average area for each condition. For decellularized ECM, HuCCA-1 (4,000 cells/ well) and KKU-213 (5,000 cells/ well) were seeded in 96-well plate to reach confluence at 48 h. Cells were incubated in warm 0.25% Trypsin–EDTA (GIBCO) for 8 min to complete cell detachment followed by aspiration of cells. Wells were rinsed twice and treated with culture medium supplemented with 10% FBS before usage.

Time-lapse and transwell cell migration assays

CCA cell migration were evaluated using two assays: time-lapse and transwell cell migration. For time-lapse analysis, cells were seeded in the 96 well black polystyrene microplate (3603; Corning Incorporated) and transfected with siLAMA3 or siNeg for 48 h as previously described. Cells were stained with Hoechst dyes (1:500) (MedChemExpress) for 15 min and the cell motility was monitored using an Operetta High-Content Imaging System (PerkinElmer) with a $40 \times$ objective lens. Fluorescence and bright field images were captured every 15 min for 12 h. Migration speed was calculated by nuclei tracking using the Columbus™ software (PerkinElmer).

For transwell migration assay, CCA cells suspension in serum-free media (10^5 cells/200 μl) was added into the apical inserts of transwell (3422; Corning Incorporated) and placed into the lower compartment filled with 600 μl of complete medium. After incubation at 37°C in a humidified 5% CO_2 incubator for 12 h, cells underneath

the upper chamber membrane were fixed with 30% methanol for 30 min and stained with 0.5% crystal violet for 10 min. Migrating cells were counted from four visual fields observed under 20× magnification of an inverted microscope.

Flow cytometry

To investigate cell death, 48-h transfected CCA cells (5×10^5 cells per well) were seeded into a 6-well plate for 24 h. Both adherent and non-adherent cells were harvested, wash twice with cold PBS and resuspended in Annexin V-binding buffer and stained with Annexin V (AV) (BioVision) and propidium iodide (PI) (Thermo Fisher Scientific) and then incubated at room temperature for 5 min in the dark. Cells (10^4) were collected using BD Accuri C6 Plus flow cytometer (BD Biosciences) and the percentage of apoptotic cells was acquired from an addition of the percentage of early (AV + /PI-) and late (AV + /PI+) apoptotic cells.

Cell cycle progression was analyzed after forty-eight-hour transfection. Cells were harvested, fixed with cold 70% ethanol at 4 °C for 2 h and then washed twice with PBS. Cells were resuspended and incubated overnight in staining buffer (PBS with 100 µg/mL RNase A, 50 µg/mL PI and 0.1% Triton X-100) at 4 °C in the dark. Flow cytometry was used to determine cell cycle phases by measuring nuclear DNA content from the intensity of PI.

Western blot analysis

Forty-eight-hour transfected KCU-213 cells were reseeded for 24 h, then proteins were extracted in lysis buffer containing 150 mM Tris-HCl pH 7.4, 150 mM NaCl, 0.1% SDS, 1% sodium deoxycholate, 1% Nonidet P-40, 50 mM NaF, 2 mM Na_3VO_4 , 40 mM β -glycerophosphate, 1 mM dithiothreitol, and a protease inhibitor cocktail (Roche). Aliquots (25 µg) of protein were resolved by 10 or 15% sodium dodecyl sulfate polyacrylamide gel electrophoresis and electrotransferred onto nitrocellulose membrane. The membranes were then incubated with primary antibodies (viz. rabbit anti-pFAK (8556), rabbit anti-E-cadherin (3195), rabbit anti-vimentin (5714), rabbit anti-Slug (9585), and rabbit anti-claudin-1 (13255) antibodies (Cell Signaling); and rabbit anti-tFAK (sc-557; Santa Cruz Biotechnology) followed by goat anti-rabbit horseradish peroxidase (HRP)-conjugated IgG secondary antibodies (7074; Cell Signaling). GAPDH was utilized to normalize gel loading and detected with mouse anti-GAPDH antibody (sc-32233; Santa Cruz Biotechnology) followed by the goat anti-mouse HRP-conjugated IgG secondary antibody (7076; Cell Signaling). Clarity Western ECL reagent (BioRad) was employed to obtain chemiluminescent signals recorded by a G-Box Chemi XL system (Syngene).

E-Cadherin, cytoskeleton staining and cell shape-descriptor analysis

48-h transfected CCA cells (1×10^4 cells per well) were seeded for 24 h onto an 8-well chamber slide (30108; SPL Life Science). Cells then were fixed with 4% paraformaldehyde for 15 min, and permeabilized with 0.5% Triton X-100 for 20 min, and then subjected to a blocking step using 1% bovine serum albumin (BSA) in PBS at room temperature for 90 min. Then, the cells were probed with E-cadherin antibody (24E10) (3195; Cell Signaling) at a dilution of 1:1,600 in 1% BSA at 4 °C overnight. The cells were probed with Alexa Fluor® 488 goat anti-rabbit antibody (A11011; Molecular Probes) at a dilution of 1:500 in 1% BSA for 1 h at room temperature. Cell nuclei and F-actin were stained for 1 h with Hoechst 33342, and phalloidin-Alexa 546 (1:1000) (Thermo Scientific). Stained cells were captured with FV1000 (Olympus Corporation) under 60× magnification.

To obtain the total area of cell spreading, the distribution area of F-actin was detected using phalloidin staining and analyzed by Image J software using the ROI (Region of Interest) manager tool, in which the individual cells were selected manually. For a group of continually attached cells, the average distribution area was calculated by dividing the total distribution area by the number of nuclei stained with Hoechst. Particles along the image border and out of focus were excluded. Finally, the data of the F-actin spreading area from single cells and a group of cells were combined and visualized in the unit area of $\mu\text{m}^2/\text{cell}$. The circularity of cells was investigated according to the following equations:

$$\text{Circularity} = \frac{4\pi A}{P^2}$$

where P is the perimeter and A is the cell area.

Statistical analysis

All statistical analyses were performed using Graphpad Prism software version 7 (GraphPad Software, Inc., San Diego, California). Mean comparisons between groups were determined using Welch's *t*-test, Wilcoxon matched-pairs signed rank or one-way ANOVA where appropriate. Data were expressed as mean ± standard error of mean (SEM) of at least three independent experiments and statistical significance was considered when *P*-value was < 0.05, unless indicated.

Data availability

The datasets analyzed in the current study are publicly available accordingly: GSE107943 (<https://www.ncbi.nlm.nih.gov/geo/query/acc.cgi?acc=GSE107943>); PCAWG (<https://www.ebi.ac.uk/gxa/experiments/E-MTAB-5423/Downloads>); TCGA-CHOL (<https://portal.gdc.cancer.gov/projects/TCGA-CHOL>); and collated microarray data were available in previous publication (<https://doi.org/10.3390/ph14090898>)⁴¹. Processed data and R-scripts generated during the current study are provided in Figshare with the identifier <https://doi.org/10.6084/m9.figshare.22332838.v1>.

Received: 20 February 2023; Accepted: 30 November 2023

Published online: 18 December 2023

References

- Banales, J. M. *et al.* Cholangiocarcinoma 2020: the next horizon in mechanisms and management. *Nat. Rev. Gastroenterol. Hepatol.* **17**, 557–588 (2020).
- Høgdall, D., Lewinska, M. & Andersen, J. B. Desmoplastic tumor microenvironment and immunotherapy in cholangiocarcinoma. *Trends Cancer* **4**, 239–255 (2018).
- Sirica, A. E. *et al.* Intrahepatic cholangiocarcinoma: Continuing challenges and translational advances. *Hepatology* **69**, 1803–1815 (2019).
- Fabris, L. *et al.* The tumour microenvironment and immune milieu of cholangiocarcinoma. *Liver Int.* **39**(Suppl 1), 63–78 (2019).
- Aumailley, M. *et al.* A simplified laminin nomenclature. *Matrix Biol.* **24**, 326–332 (2005).
- Belkin, A. & Stepp, M. Integrins as Receptors for Laminins.pdf. *Microsc. Res. Tech.* **51**, 280–3011 (2002).
- Givant-Horwitz, V., Davidson, B. & Reich, R. Laminin-induced signaling in tumor cells. *Cancer Lett.* **223**, 1–10 (2005).
- Ribatti, D., Tamma, R. & Annesse, T. Epithelial-mesenchymal transition in cancer: A historical overview. *Transl. Oncol.* **13**, 100773 (2020).
- Fabris, L., Cadamuro, M., Cagnin, S., Strazzabosco, M. & Gores, G. J. Liver matrix in benign and malignant biliary tract disease. *Semin. Liver Dis.* **40**, 282–297 (2020).
- Islam, K., Thummarati, P., Kaewkong, P., Sriya, B. & Suthiphongchai, T. Role of laminin and cognate receptors in cholangiocarcinoma cell migration. *Cell. Adhes. Migr.* **15**, 152–165 (2021).
- Liao, C. H. *et al.* microRNA-329 suppresses epithelial-to-mesenchymal transition and lymph node metastasis in bile duct cancer by inhibiting laminin subunit beta 3. *J. Cell. Physiol.* **234**, 17786–17799 (2019).
- Aishima, S. *et al.* Biliary neoplasia with extensive intraductal spread associated with liver cirrhosis: A hitherto unreported variant of biliary intraepithelial neoplasia. *Hum. Pathol.* **39**, 939–947 (2008).
- Liu, W. *et al.* Aberrant expression of laminin γ 2 correlates with poor prognosis and promotes invasion in extrahepatic cholangiocarcinoma. *J. Surg. Res.* **186**, 150–156 (2014).
- Rousselle, P. & Scoazec, J. Y. Laminin 332 in cancer: When the extracellular matrix turns signals from cell anchorage to cell movement. *Semin. Cancer Biol.* (2019).
- Xu, C. Y. *et al.* SphK1 modulates cell migration and EMT-related marker expression by regulating the expression of p-FAK in colorectal cancer cells. *Int. J. Mol. Med.* **39**, 1277–1284 (2017).
- Sirica, A. E. & Gores, G. J. Desmoplastic stroma and cholangiocarcinoma: Clinical implications and therapeutic targeting. *Hepatology (Baltimore, Md.)* **59**, 2397–2402 (2014).
- Pouliot, N. & Kusuma, N. Laminin-511: A multi-functional adhesion protein regulating cell migration, tumor invasion and metastasis. *Cell Adhes. Migr.* **7**, 142–149 (2013).
- Utispan, K. *et al.* Gene expression profiling of cholangiocarcinoma-derived fibroblast reveals alterations related to tumor progression and indicates periostin as a poor prognostic marker. *Mol. Cancer* **9**, 13–32 (2010).
- Zhang, H. *et al.* LAMB3 mediates apoptotic, proliferative, invasive, and metastatic behaviors in pancreatic cancer by regulating the PI3K/Akt signaling pathway. *Cell Death Dis.* **10**, 230 (2019).
- Srisomsap, C. *et al.* Proteomic studies of cholangiocarcinoma and hepatocellular carcinoma cell secretomes. *J. Biomed. Biotechnol.* **2010**, 437143 (2010).
- Pei, Y. F., Liu, J., Cheng, J., Wu, W. D. & Liu, X. Q. Silencing of LAMC2 reverses epithelial-mesenchymal transition and inhibits angiogenesis in cholangiocarcinoma via inactivation of the epidermal growth factor receptor signaling pathway. *Am. J. Pathol.* **189**, 1637–1653 (2019).
- Tang, Z., Kang, B., Li, C., Chen, T. & Zhang, Z. GEPIA2: An enhanced web server for large-scale expression profiling and interactive analysis. *Nucleic Acids Res.* **47**, W556–w560 (2019).
- Moller-Levet, C. S. *et al.* Exon array analysis of head and neck cancers identifies a hypoxia related splice variant of LAMA3 associated with a poor prognosis. *PLoS Comput. Biol.* **5**, e1000571 (2009).
- Caley, M. P. *et al.* Loss of the laminin subunit alpha-3 induces cell invasion and macrophage infiltration in cutaneous squamous cell carcinoma*. *Br. J. Dermatol.* **184**, 923–934 (2021).
- Aumailley, M. The laminin family. *Cell Adhes. Migr.* **7**, 48–55 (2013).
- Huang, C. & Chen, J. Laminin-332 mediates proliferation, apoptosis, invasion, migration and epithelial-to-mesenchymal transition in pancreatic ductal adenocarcinoma. *Mol. Med. Rep.* **23**, 11 (2021).
- Zhou, B., Moodie, A., Blanchard, A. A. A., Leygue, E. & Myal, Y. Claudin 1 in breast cancer: New insights. *J. Clin. Med.* **4**, 1960–1976 (2015).
- Thummarati, P. *et al.* High level of urokinase plasminogen activator contributes to cholangiocarcinoma invasion and metastasis. *World J. Gastroenterol.* **18**, 244–250 (2012).
- Menakongka, A. & Suthiphongchai, T. Involvement of PI3K and ERK1/2 pathways in hepatocyte growth factor-induced cholangiocarcinoma cell invasion. *World J. Gastroenterol.* **16**, 713–722 (2010).
- Treekitkarnmongkol, W. & Suthiphongchai, T. High expression of ErbB2 contributes to cholangiocarcinoma cell invasion and proliferation through AKT/p70S6K. *World J. Gastroenterol.* **16**, 4047–4054 (2010).
- Yang, X. H. *et al.* Disruption of laminin-integrin-CD151-focal adhesion kinase axis sensitizes breast cancer cells to ErbB2 antagonists. *Cancer Res.* **70**, 2256–2263 (2010).
- Islam, K. *et al.* Bioinformatics and qPCR analyses of laminins' cognate receptors in cholangiocarcinoma tissues reveal the integrin ITGB4 as a potential biomarker. *Sci. Asia* **48**, 379–386 (2022).
- Chung, L. M. *et al.* Differential expression analysis for paired RNA-seq data. *BMC Bioinf.* **14**, 110 (2013).
- Islam, S. *et al.* ITGA2, LAMB3, and LAMC2 may be the potential therapeutic targets in pancreatic ductal adenocarcinoma: An integrated bioinformatics analysis. *Sci. Rep.* **11**, 10563 (2021).
- Yang, C. *et al.* Evaluation of the diagnostic ability of laminin gene family for pancreatic ductal adenocarcinoma. *Aging (Albany NY)* **11**, 3679–3703 (2019).
- Sriya, B. *et al.* Establishment and characterization of an opisthorchiasis-associated cholangiocarcinoma cell line (KKU-100). *World J. Gastroenterol.* **11**, 3392–3397 (2005).
- Sriya, B. *et al.* Functional and genetic characterization of three cell lines derived from a single tumor of an Opisthorchis viverrini-associated cholangiocarcinoma patient. *Hum. Cell* **33**, 695–708 (2020).
- Maruyama, M. *et al.* Establishment of a highly differentiated immortalized human cholangiocyte cell line with SV40T and hTERT. *Transplantation* **77**, 446–451 (2004).
- Sirisinha, S. *et al.* Establishment and characterization of a cholangiocarcinoma cell line from a Thai patient with intrahepatic bile duct cancer. *Asian Pac. J. Allergy Immunol.* **9**, 153–157 (1991).
- Weinstein, J. N. *et al.* The cancer genome atlas pan-cancer analysis project. *Nat. Genet.* **45**, 1113–1120 (2013).
- Campbell, P. J. *et al.* Pan-cancer analysis of whole genomes. *Nature* **578**, 82–93 (2020).

42. Balasubramanian, B. *et al.* RTK25: A comprehensive molecular profiling strategy in cholangiocarcinoma using an integrated bioinformatics approach. *Pharmaceuticals* **14**, (2021).
43. Puetkasichonpasutha, J., Namwat, N., Sa-Ngiamwibool, P., Titapun, A. & Suthiphongchai, T. Evaluation of p53 and its target gene expression as potential biomarkers of cholangiocarcinoma in thai patients. *Asian Pac. J. Cancer Prev.* **21**, 791–798 (2020).
44. Yang, J., Yang, Q., Yu, S. & Zhang, X. Evaluation and validation of suitable reference genes for reverse transcription-quantitative polymerase chain reaction studies in cholangiocarcinoma patients and cell lines. *Oncol. Lett.* **11**, 2673–2681 (2016).
45. Chen, E.Y. *et al.* Enrichr: interactive and collaborative HTML5 gene list enrichment analysis tool. *BMC Bioinform.* **14**, 128 (2013).
46. Kuleshov, M.V. *et al.* Enrichr: a comprehensive gene set enrichment analysis web server 2016 update. *Nucleic Acids Res.* **44**, W90–W97 (2016).
47. Xie, Z. *et al.* Gene set knowledge discovery with Enrichr. *Curr. Protoc.* **1**, e90 (2021).
48. Kanehisa, M. & Goto, S. KEGG: Kyoto encyclopedia of genes and genomes. *Nucleic Acids Res.* **28**, 27–30 (2000).

Acknowledgements

This work was funded by the Basic Research Funding: Fiscal year 2021, Mahidol University, Grant number: BRF2-NDFR21/2564. This research was supported by The Central Instrument Facility (CIF) Grant, Faculty of Science, Mahidol University and BB has been conducted under postdoctoral research sponsorship of Mahidol University.

Author contributions

K.I.: Conceptualization, Methodology, Validation, Formal analysis, Investigation, Writing—original draft preparation, Writing—review and editing; B.B., and S.V.: Data curation, Validation, Formal analysis and Investigation, Writing—original draft preparation; P.T.: Investigation, Formal analysis, Visualization; J.T., N.P. T.K., and P.K. (Pornparn Kongpracha), and Y.K.: Investigation; P.K. (Phongthon Kanjanasirirat): Formal analysis; T.J.: Funding acquisition; P.W., S.B. and N.N.: Resource; R.T.: Supervision, Resources; T.S.: Conceptualization, Methodology, Validation, Writing—review and editing, Funding acquisition, Resources, Supervision.

Competing interests

The authors declare no competing interests.

Additional information

Supplementary Information The online version contains supplementary material available at <https://doi.org/10.1038/s41598-023-48798-8>.

Correspondence and requests for materials should be addressed to T.S.

Reprints and permissions information is available at www.nature.com/reprints.

Publisher's note Springer Nature remains neutral with regard to jurisdictional claims in published maps and institutional affiliations.



Open Access This article is licensed under a Creative Commons Attribution 4.0 International License, which permits use, sharing, adaptation, distribution and reproduction in any medium or format, as long as you give appropriate credit to the original author(s) and the source, provide a link to the Creative Commons licence, and indicate if changes were made. The images or other third party material in this article are included in the article's Creative Commons licence, unless indicated otherwise in a credit line to the material. If material is not included in the article's Creative Commons licence and your intended use is not permitted by statutory regulation or exceeds the permitted use, you will need to obtain permission directly from the copyright holder. To view a copy of this licence, visit <http://creativecommons.org/licenses/by/4.0/>.

© The Author(s) 2023